Theoretical and Experimental Evidence for a Nodal Energy Gap in MgB_2

Y. Dan Agassi[a] and Daniel E. Oates[b]

[a]Consultant, Jerusalem, Israel

[b]MIT Lincoln Laboratory, 244 Wood St., Lexington, MA 02420 USA

Abstract

We present a phenomenological model that indicates with high probability that the smaller of the two energy gaps in MgB_2, the so-called π gap, contains nodal lines with a six-fold symmetry (i-wave). The model also indicates that the larger gap, the so-called σ gap, is a conventional s wave. The model is an extension of the BCS theory that accounts for the elastic anisotropy in MgB_2 and the Coulomb repulsion. It is based on a phononic pairing mechanism and assumes no coupling between the two energy gaps in MgB_2 at zero temperature. All of the parameters of the model, such as the sound velocities, are independently determined material constants. The results agree with a previous ad-hoc hypothesis that the π energy gap has six nodal lines. That hypothesis was motivated by low-temperature measurements of the surface impedance and intermodulation distortion in high-quality thin films. We briefly review experimental evidence in support of our hypothesis and review evidence in the literature that has led to the conclusion that both gaps are s wave. We find that the evidence from the literature for s wave is inconclusive. Our finding is that the π gap has six nodal lines.

Key words

Magnesium diboride, energy-gap symmetry, surface impedance, microwave resonators, superconducting thin films, pairing symmetry

Corresponding author: Daniel E. Oates, email:oates@ll.mit.edu; oates314@gmail.com Tel: 781.981.4707

Distribution A: Public Release, unlimited distribution. This material is based upon work supported by the Department of the Navy under Air Force Contract No. FA8721-05-C-0002 and/or FA8702-15-D-0001. Any opinions, findings, conclusions or recommendations expressed in this material are those of the authors and do not necessarily reflect the views of the Department of the Navy.

1 Introduction

Superconducting magnesium diboride has been demonstrated to possess properties that are promising for applications at microwave frequencies. The relatively high transition temperature of 40 K, low surface resistance, relatively long coherence length, and the high critical magnetic field of >1 T have led to interest for microwave electronic applications, such as filters and for superconducting radio frequency (SRF) applications in accelerator cavities[1]. MgB_2 has also attracted fundamental interest because of the two superconducting energy gaps, while at the same time it appears to be a superconductor where the pairing mechanism is phononic as in BCS theory [1,2].

In investigations of the microwave-frequency properties of high-quality thin films of MgB_2, we have previously found strong evidence that the smaller of the energy gaps has a symmetry that includes nodal lines, and the symmetry is six fold ($\boldsymbol{\ell} = 6$, i-wave in spectroscopic notation) due to the hexagonal crystal structure of MgB_2,

$$\Delta_\pi(\varphi;T) = \Delta_\pi(T)\sin(6\varphi), \tag{1}$$

where $\Delta_\pi(T)$ is the π energy-gap magnitude and φ denotes the azimuthal angle in the cylindrical-coordinate system of the relative k-space. This proposition has been reported in series of papers[3,4,5]. These findings will be discussed in more detail in Section II. Recently, measurements of the microwave properties of MgB_2 by another group [6], using a different method and with different high-quality films, have been reported. As the analysis in Section II demonstrates, this experimental evidence agrees with the $\boldsymbol{\ell} = 6$ hypothesis, while inconsistent with s-wave symmetry.

To give the $\boldsymbol{\ell} = 6$ hypothesis a theoretical underpinning, we have developed a phenomenological model for calculating the energy gaps in MgB_2 at $T = 0$ K. The presentation of this model is the main purpose of this work. The results strongly support the hypothesis that the smaller gap, the so-called π gap, exhibits $\boldsymbol{\ell} = 6$ symmetry while the larger gap, the σ gap, has conventional s-wave symmetry. The model is parameter-free, meaning that all parameters used are available from other calculations or measurements in the literature. The model is inspired by previous work regarding the d-wave symmetry of the energy-gap of YBCO, a cuprate [7]. This work builds on a previous generalization of the BCS theory, where the coulomb repulsion is included [8], and adds the important feature of large anisotropy in the elastic properties. Our work differs from [7], however, in several respects. It is applied to MgB_2 where the pairing mechanism is believed to be phononic [9,10,11], the attractive interaction parametrization is distinct, and it aims at the $T = 0$ K energy gap rather than a focus on the $T \sim T_C$ domain

We are aware that it has been widely concluded in the literature that both energy gaps of MgB_2 have a conventional s-wave symmetry. In the discussion, Section IV, we examine literature for probes that imply the π energy-gap symmetry. Our finding is that the pertaining literature that suggests the s-wave symmetry is inconclusive and hence the proposition of a $\boldsymbol{\ell} = 6$

symmetry for π energy gap is not inconsistent with the literature. In that Section it is also speculated on other instances where the i-wave energy gap symmetry may be realized and propose further experimental work to settle the symmetry proposition of this work.

2 Review of the evidence for $\ell = 6$

2.1 Intermodulation Distortion

As reported previously [3], microwave measurements of the temperature dependence of the intermodulation distortion (IMD) in MgB_2 at low temperatures show a $1/T^2$ increase as the temperature is lowered. As a reminder, Figure 1 shows this previously reported result, where the similar data from YBCO is included [12].

The $1/T^2$ behavior in YBCO is attributed to the nonlinear Meissner effect [13,14]. It is a signature of a nodal energy gap, a d-wave in the case of YBCO. In analogy to YBCO case, we have interpreted the observed low-temperature increase in IMD in MgB_2 as a strong indication that the energy gap contains nodal lines. As discussed in detail in Section III, the hexagonal crystal symmetry of MgB_2 and the observed $1/T^2$ behavior of IMD(T) implies the $\ell = 6$ symmetry. For an s-wave energy-gap symmetry the IMD vanishes exponentially as $T \rightarrow 0$ K. No other plausible explanation has been offered for the measured IMD(T).

2.2 Penetration Depth $\Delta\lambda(T)$

Another piece of evidence for the $\ell = 6$ symmetry is the low-temperature variation of the penetration depth reported and analyzed in Ref.[4]. Below the temperature of about 5 K the penetration depth increases as the temperature is lowered. Figure 2 shows the result reported in Ref [4] of fits that assume $\ell = 6$ symmetry for the dominating π energy gap. We have interpreted the increase as a manifestation of Andreev surface-attached states that are associated with the existence of nodal lines in the energy gap. An identical observation was reported for YBCO, which has nodal d-wave energy-gap symmetry with two nodal lines [15, 16].

2.3 Surface Resistance vs Temperature $R_s(T)$

The temperature dependence of the surface resistance $R_s(T)$ also sheds light on the symmetry of the energy gap. As discussed in the following, for s-wave symmetry $R_s(T)$ vanishes exponentially as the temperature is lowered, while for a nodal energy gap it follows a power law. Our data shows indeed a power-law temperature variation at low temperatures, consistent with the $\ell = 6$ premise [5]. Recently, measurements [6] of the $R_s(T)$ for high-quality MgB_2 films from a different source from that of [3,4] and by a different measurement method have been published by a group at Jefferson National Accelerator Facility (JLab). As demonstrated in the following, our new analysis of these measurements confirms that they too support the $\ell = 6$ hypothesis.

The presumed symmetry of the MgB_2 σ energy gap as an s-wave [1] implies that at sufficiently low temperatures the π energy gap dominates the temperature dependence. Hence, in

the low-temperature domain and in the clean limit, an s-wave π energy gap yields a surface-resistance R_S that obeys the BCS-theory textbook expression that is characterized by an exponential temperature dependence, specifically,[17,18]

$$R_S(T) = R_{RES} + C\, f^2 \beta\, e^{-\Delta(T)\beta}\,. \qquad (2)$$

In Eq. (2) f is the frequency, $\beta = 1/(k_B T)$ where k_B is the Boltzmann constant and R_{RES}, C are temperature-independent fitting parameters of the residual surface resistance and a proportionality factor, respectively. The quantity R_{RES} is experimentally extracted from the very-low temperature surface-resistance data, where no measurable temperature dependence is observed. The origin of this term is presumed not related to bulk superconductivity [19]. Details of the JLab experiments have been given elsewhere [6]. In brief, the measured single-crystal MgB_2 films were grown by the HPCVD method [1], and have been measured in a TE_{011} cylindrical Nb cavity with a sapphire rod inside. The resonant frequency is 7.4 GHz. The analysis of the loss and shift in resonance frequency in this setup yields the effective surface-resistance and penetration-depth dependencies on temperature.

The $R_S(T)$ expression in Eq. (2) suggests a semi-log plot vs.$1/T$. In such a plot, data that conforms to Eq.(2) would lie along a straight line with slope proportional to $\Delta_\pi(T = 0\ \mathrm{K}) \approx 2.3$ meV, the accepted value for the π energy gap [1,2,20]. The plot in Figure 3) shows for clarity only the results for the 350-nm-thick film from [6]. Similar results are obtained for the 200-nm-thick film. This figure convincingly shows that the data does not follow the expected straight line for an assumed s-wave energy gap value $\Delta_\pi(T = 0\ \mathrm{K}) \approx 2.3$ meV. As a consistency check to the analysis of the R_S data in Figure 3), we plot in Figure 4) the Nb data, also reported by the JLab group [6]. As expected, the BCS expression fits the low-temperature data using the literature value of the Nb energy gap, $\Delta_{Nb}(T = 0\ \mathrm{K}) = 1.5$ meV [21] for about two orders of magnitude.

The inconsistency of the low-temperature surface-resistance data with the BCS expression, Eq.(1), demonstrated in Figure 3) is resolved by analyzing the data under the previously proposed assumption that the π energy gap has a symmetry with six nodal lines, Eq.(1). This energy-gap symmetry yields for the surface resistance [3]

$$R_S(T) = R_{RES} + a\left(\frac{1}{\bar{\beta}} + \left(\frac{15}{8}\right)\frac{1}{\bar{\beta}^3}\right), \qquad \bar{\beta} = \frac{\Delta_\pi(T = 0K)}{k_B T}, \qquad (3)$$

where $a > 0$ and R_{RES} are defined above. Since at low temperatures the variation of $\Delta_\pi(T)$ is negligible we approximate in Eq. (3) $\Delta_\pi(T) \approx \Delta_\pi(T = 0\ \mathrm{K})$ [20]. The expression in Eq. (3) is based on the two-fluid model, where at low temperatures the temperature variation reflects primarily the corresponding temperature variation of the quasiparticle density [21]. Note the qualitatively

distinct temperature variations of expressions Eq. (2) and Eq. (3), an exponential vs. a power-law.

Figure 5) shows the results of fitting the $R_S(T)$ - R_{RES} of the 350-nm-thick film from JLab with the expression in Eq.(3). For comparison, measurements made with stripline resonators at MIT Lincoln Laboratory are also plotted [22]. In order to plot the stripline data at f = 2.2 GHz and the Jlab data at f = 7.4 GHz on the same graph, the MIT Lincoln Laboratory measurement was scaled by the usual f^2 dependence. The Lincoln Laboratory measurements are of a film deposited by reactive evaporation [23] and unpublished measurements of a film deposited by HPCVD process which is also the case for the films measured at JLab. As Figure 5) demonstrates, the fits are very good in all cases. The fits, however, show variability in slope and fitting parameters. Such variability has its probable origin in uncontrolled factors in the film deposition method, and is normal in measurements of superconducting thin films. The point of Figure 5) is that regardless of such extraneous uncontrolled factors, all films share the same particular temperature variation of Eq. (3). This outcome resolves the inconsistency encountered in Figure 3). We emphasize that the Jlab measurements and above analysis are not a stand-alone proof of the unconventional energy-gap symmetry, Eq. (1), but rather provide additional support to the original proposition that was based on measurement of the IMD [3]. Accounting for the σ energy-gap contribution at higher temperatures lies outside the scope of this work.

3 Phenomenological model for the energy-gap symmetry

In this Section we show that the $\ell = 6$ energy-gap symmetry, Eq. (1), is also substantiated by calculations based on a phenomenological model. That model was introduced for and successfully applied to YBCO [7], where d-wave symmetry of the energy gap is supported by a large body of data [24]. The model is based on a phononic-pairing-mechanism premise, which is generally accepted to be the case for MgB_2 [9]. It generalizes the classic BCS theory in two respects. It accounts for the mutual Coulombic repulsion between the two electrons in a Cooper pair [8] and for anisotropy in the superconductor elastic properties In YBCO [7] and MgB_2 this anisotropy is substantial, see below. All the required input parameters are extracted from pertaining calculations and data in the literature.

A complication in MgB_2 that is absent in YBCO is the existence of two energy gaps, the π (small) and σ (large) energy gaps, respectively. These are weakly coupled due to their distinct underlying bonding. At temperatures $T \sim T_C$ however, where the energy gaps become small [25, 26, 27], this coupling cannot be ignored. By contrast in the $T \to 0$ K limit, it can be neglected given the considerable disparity in the energy gap magnitudes $\Delta_\pi(T=0) \approx 0.002$ eV, $\Delta_\sigma(T=0) \approx 0.007$ eV . Consequently, at $T = 0$ K the two energy gaps can be treated separately, a feature that simplifies the analysis considerably.

Our objective is solving the general BCS energy-gap equation at $T = 0$ K,

$$\Delta\left(\vec{k}\right) = -\sum_{\vec{k}'} V\left(\vec{k},\vec{k}'\right)\frac{\Delta\left(\vec{k}'\right)}{2E\left(\vec{k}'\right)} \to -\frac{\boldsymbol{\mathcal{V}}}{(2\pi)^3}\int_{BZ} d\vec{k}'\, V\left(\vec{k},\vec{k}'\right)\frac{\Delta\left(\vec{k}'\right)}{2E\left(\vec{k}'\right)} \qquad (4)$$
$$E\left(\vec{k}'\right) = \sqrt{\left(\xi\left(\vec{k}'\right)\right)^2 + \left|\Delta\left(\vec{k}'\right)\right|^2}, \qquad \xi\left(\vec{k}'\right) = \varepsilon\left(\vec{k}'\right) - \mu.$$

The symbols in Eq.(4) denote the following. The energy gap at $T = 0$ K is $\Delta\left(\vec{k}\right)$, the momentum is $\vec{k}$ and the summation (integration) is over the first Brillouin zone, denoted by *BZ*. The sample volume is $\boldsymbol{\mathcal{V}}$, the chemical potential is μ, and the band-energy and quasiparticle energy are $\varepsilon\left(\vec{k}\right)$ is $E\left(\vec{k}\right)$, respectively. The mutual interaction of the two electrons in a Cooper pair is $V\left(\vec{k},\vec{k}'\right)$ [28].Eq.(4) has always the trivial solution, $\Delta\left(\vec{k}\right) = 0$, which corresponds to a state without quasiparticles [28]. We are interested, however, only in nontrivial solutions where $\Delta\left(\vec{k}\right) \neq 0$, if they exist. Technical details of solving Eq.(4) are deferred to the Appendices. In this Section, we focus only on key ingredients of the model and results of the calculations. In the BCS theory, where $\Delta\left(\vec{k}\right)$ and $V\left(\vec{k},\vec{k}'\right)$ are assumed to be constants, the nontrivial solution of Eq.(4) can be found in textbooks [21, 29].

Consider first the interaction factor $V\left(\vec{k},\vec{k}'\right)$ in Eq.(4). It consists of an attraction, resulting from a single-phonon exchange, and the corresponding Coulomb repulsion. When accounting for realistic phonon modes, this interaction factor is complex [30]. Here we follow the generalized BCS theory by adopting the following ansatz [31, 7]

$$V\left(\vec{k},\vec{k}'\right) = \frac{1}{\boldsymbol{\mathcal{V}}}V_{PH}\left(\vec{q}\right)\theta\left(\hbar\omega_D - \left|\xi\left(\vec{k}\right)\right|\right)\theta\left(\hbar\omega_D - \left|\xi\left(\vec{k}'\right)\right|\right)$$
$$+\frac{1}{\boldsymbol{\mathcal{V}}}V_C\left(\vec{q}\right)\theta\left(\hbar\omega_P - \left|\xi\left(\vec{k}\right)\right|\right)\theta\left(\hbar\omega_P - \left|\xi\left(\vec{k}'\right)\right|\right) \equiv \mathrm{V}\left(\vec{q},\left|\xi\left(\vec{k}\right)\right|,\left|\xi\left(\vec{k}'\right)\right|\right), \qquad (5)$$
$$\vec{q} = \vec{k} - \vec{k}'.$$

The symbols in Eq. (5) denote the following. The interactions $V_{PH}\left(\vec{q}\right)$ and $V_C\left(\vec{q}\right)$ denote the attractive interaction due to a single phonon exchange between the two Cooper-pair electrons and corresponding Coulombic repulsion, respectively, ω_D and ω_P denote the Debye and plasma

frequencies, respectively, and $\theta(\xi)$ is the dimensionless step function which equals 1 or 0 for positive or negative $\xi(\vec{k})$, respectively. The step function in Eq. (5) expresses the BCS premise that only electrons within a thin energy shell near the Fermi surface partake in pairing. That energy-shell width is the Debye energy. Similarly, the maximum energy exchanged due to the Coulomb repulsion is the plasma energy [8,31]

Consider first the attractive interaction $V_{PH}(\vec{q})$ in Eq. (5). For an isotropic superconductor in the weak-coupling regime, the single-phonon attractive interaction is given by [32]

$$V_{PH} = -\gamma^2 \theta(\hbar\omega_D - \hbar\omega), \qquad \gamma = \left(\frac{z e^2}{v_{SOUND}}\right)\left(\frac{4\pi}{q_{TF}^2}\right)\sqrt{\frac{n_0}{M}} = \frac{\pi^2 (\hbar c)^3 z}{(m^* c^2)^2 \left(\frac{v_F}{c}\right)}\left(\frac{n_0}{\sqrt{B}}\right) \qquad (6)$$

where γ is a constant amplitude (dimensionality $[\gamma] = \sqrt{\mathcal{E}}\,\ell^{3/2}$ with $\mathcal{E}$ and ℓ denoting energy and length, respectively) and $\hbar\omega$ is the exchanged-phonon energy. The other symbols in Eq(6) denote the following: z is the partaking-ion valency, v_{SOUND} is the *longitudinal* sound velocity, q_{TF} is the Thomas-Fermi momentum. The n_0 parameter is the ion number density (dimensionality $[n_0] = \ell^{-3}$), i.e., zen$_0$ is the ionic-background charge density that neutralizes the electron-sea charge density. The M parameter is the partaking-ion mass and B is the bulk modulus (dimensionality $[B] = \mathcal{E}\ell^{-3}$). The second expression for γ in Eq.(6) is obtained by employing the spherical Fermi-sea expressions $q_{TF}^2 = (6\pi n_0 e^2)/\varepsilon_F$, $\varepsilon_F = \hbar^2 k_F^2/(2m^*)$, $k_F = (6\pi^2 n_0/2)^{1/3}$ and $(v_{SOUND})^2 = B/(M n_0)$ where m^* denotes the effective electron mass. It provides a connection of γ with measurable or calculated quantities in the literature. Eq. (6) is based on the standard jelium model for metals, a system comprising a positive ionic-charge background, z e n$_0$ that is compensated by the Fermi-sea charge-density of electrons released by the ions. Note that in the relative distance between the two Cooper-pair electrons, the interaction Eq. (6), is a delta function.

The point to note in Eq.(6) is the v_{SOUND} (or B) factor, which in general depends on the direction in momentum space. That directional dependence reflects the disparity in the crystal elastic constants [33]. For a hexagonal crystal structure in particular, the longitudinal sound velocities in the xy plane and in the $\hat{z}$ direction are given by [34]

$$v_{SOUND}(\square)=\sqrt{\frac{C_{1,1}}{\rho}},\qquad v_{SOUND}(\perp)=\sqrt{\frac{C_{3,3}}{\rho}}, \tag{7}$$

where $C_{1,1}, C_{3,3}$ are the elastic constants in the standard notation (dimensionality $\left[C_{i,j}\right]=\mathcal{E}\,\ell^{-3}$) and ρ is the ion mass-density (dimensionality $[\rho]=\mathcal{E}\mathrm{t}^{2}\ell^{-5}$, where t denotes time). In Eq.(7) and hereafter the symbols $\square$ and $\perp$ denote quantities pertaining to the basal plane and z directions in the cylindrical coordinate system, respectively. A large disparity between $C_{1,1}$ and $C_{3,3}$ implies a corresponding significant $\vec{q}$-dependence of the interaction V_{PH}. Deferring details to the Appendices, the parametrization of this dependence is a key ingredient of our model. Specifically we use

$$V_{PH}(\vec{q})=-\frac{1}{1+\alpha\left(\frac{q_{\square}^{2}}{q^{2}}\right)}\times\begin{Bmatrix}\gamma_{\pi}^{2}\\ \gamma_{\sigma}^{2}\end{Bmatrix}\begin{cases}for\ \pi\ gap\\ for\ \sigma\ gap\end{cases},\qquad q^{2}=q_{\square}^{2}+q_{\perp}^{2},$$

$$\gamma_{\pi}=\frac{\pi^{2}(\hbar c)^{3}z_{\pi}(n_{0})_{\pi}}{\left(m_{\pi}^{*}c^{2}\right)^{2}\left(\frac{v_{F}}{c}\right)_{\pi}\sqrt{B(\perp)}},\qquad \gamma_{\sigma}=\sqrt{\frac{v_{SOUND}(\perp)}{v_{SOUND}(\square)}}\frac{\pi^{2}(\hbar c)^{3}z_{\sigma}(n_{0})_{\sigma}}{\left(m_{\sigma}^{*}c^{2}\right)^{2}\left(\frac{v_{F}}{c}\right)_{\sigma}\sqrt{B(\square)}}, \tag{8}$$

where the important anisotropy parameter α is defined [7]

$$\alpha=\left(\frac{v_{SOUND}(\square)}{v_{SOUND}(\perp)}\right)^{2}-1. \tag{9}$$

In Eq.(8) $B(\perp), B(\square)$ are corresponding bulk moduli. Note that unlike for the s-wave case, in the distance between the two Cooper-pair electrons the interaction (8) is of finite range. As Eq.(9) implies, for an isotropic superconductor the anisotropy parameter vanishes.

The $V_{C}(\vec{q})$ factor in the interaction (5) is the Coulomb repulsion between the two Cooper-pair electrons. In keeping with the jelium model for metals, we adopt the standard Thomas-Fermi expression,

$$V_{C}(\vec{q})=\frac{4\pi e^{2}}{q_{TF}^{2}+q^{2}}=\gamma_{C}^{2}\left(\frac{2K_{F}^{2}}{q_{TF}^{2}+q^{2}}\right),\quad \gamma_{C}^{2}=\frac{2\,\pi\,e^{2}}{K_{F}^{2}},\quad K_{F}^{2}=\begin{cases}K_{F}^{2}(\pi) & for\ \pi\ gap\\ K_{F}^{2}(\sigma) & for\ \sigma\ gap\end{cases}, \tag{10}$$

where the basal-plane Fermi-momentum $K_F(\pi)$, $K_F(\sigma)$ refer to the π and σ energy gaps, respectively. While in principle there are four sheets to the Fermi surface [9,35], in our model we adopt just two representative Fermi-surface sheets, one for each energy gap.

Consider now the energy gap $\Delta(\vec{k})$ in Eq.(4). It is important to note that its functional dependence is severely constrained by the crystal-structure symmetry. As listed in Table 1 [36], for the hexagonal crystal structure the only allowable multipoles (in the cylindrical-coordinates basal angle) are $l = 0,3,6$. Consequently, the generalized ansatz for the gap function in the notation of Table 1 is [7]

$$\Delta\left(\vec{k}\right) = f_\Gamma\left(k_Z\right) g_\Gamma(\varphi)\left(\Delta_m^{(1)}(T)\,\theta\left(\hbar\omega_D - \left|\xi\left(\vec{k}\right)\right|\right) + \Delta_m^{(2)}(T)\,\theta\left(\hbar\omega_P - \left|\xi\left(\vec{k}\right)\right|\right)\theta\left(\left|\xi\left(\vec{k}\right)\right| - \hbar\omega_D\right)\right)$$

$$f_\Gamma\left(k_Z\right) = \begin{cases} \left\{1,\ \left(k_Z/k_{BZ}\right)^2\right\} & for\ \Gamma_1^+ \\ 1 & for\ \Gamma_2^+ \\ k_Z/k_{BZ} & for\ \Gamma_3^+ \end{cases} \qquad g_\Gamma\left(k_Z\right) = \begin{cases} 1 & for\ \Gamma_1^+ \\ \sin(6\varphi) & for\ \Gamma_2^+ \\ \left\{\sin(3\varphi), \cos(3\varphi)\right\} & for\ \Gamma_3^+ \end{cases} \tag{11}$$

where φ denotes basal-plane angle of $\vec{k}$ in a cylindrical coordinate system. As the step functions in (11) indicate, the gap $\Delta_m^{(1)}(T)$ is associated with the attractive phonon-exchange interaction. This quantity is identified with the measured energy gap. The second high-energy gap $\Delta_m^{(2)}(T)$ in Eq. (11) is associated with the Coulombic repulsion in Eq. (5). In the classic BCS theory $f_\Gamma\left(k_Z\right) = g_\Gamma(\varphi) = 1$ and $\Delta_m^{(2)}(T) = 0$. In its generalization that includes a constant coulomb interaction [8], we have $f_\Gamma\left(k_Z\right) = g_\Gamma(\varphi) = 1$ and $\Delta_m^{(2)}(T) \neq 0$, while in the present calculations $f_\Gamma\left(k_Z\right), g_\Gamma(\varphi)$ have specified functional forms dictated by the crystal structure symmetry and $\Delta_m^{(2)}(T) \neq 0$. It is expected, and numerically verified below, that $\Delta_m^{(1)}(T) \square \left|\Delta_m^{(2)}(T)\right|$ in our calculations. Note that by virtue of Eq.(11) the unknowns in the gap equation Eq. (4) are reduced to constants.

Having specified the interaction, Eqs. (8) and (10), and the allowable functional dependence of the energy gap Eq. (11), determination of the pertaining input parameters remains. These are taken from the literature and cited in Table 2. A few comments are in order before presenting the results. The first concerns the elastic constants of MgB_2. To the best of our knowledge they have not been measured [37]; however, there are calculated values based on known band-structure calculations, where the quoted values vary depending on the methods of calculation used [38]. Given this situation, we adopted for our calculations average values, specifically

$$\{C_{1,1}, C_{1,2}, C_{1,3}, C_{3,3}\} = \{444.3,\ 60.1,\ 40.3,\ 240.8\}\,\text{GPa}. \tag{12}$$

Employing these elastic constants, Eqs.(7) and (9) yield for the anisotropy parameter $\alpha = 0.84$, comparable to that in YBCO [7].

The other comments pertain to the simplified Brillouin zone and ionic parameters in Eq.(8). Underlying our approximation of no coupling between the π and σ energy gaps is the premise that the phonons responsible for these two energy gaps are distinct [10], as are the corresponding electron seas. Indeed, the calculated electron density is accumulated either around the B or Mg atoms [9]. Band structure calculations indicate that σ energy gap is associated with vibration of the B atoms in their graphitic planes, in the direction, whereas the π energy-gap is associated with vibrations that involve the Mg atoms, in the $\perp$ direction [10]. This consideration implies the choice for the participating ions' valency parameter *z* and their density n_0. A choice for the MgB_2 unit cell is a hexagon, where the Mg atoms are located at all its corners and at the centers of the hexagon's top and bottom facets. In that hexagon, the B atoms lie in a hexagonal loop located in a plane midway between the hexagon's top and bottom facets. A corresponding primitive unit-cell is a sixth of that hexagon, of volume $0.25\sqrt{3}\, a_a^2 a_c$ where a_a and a_c are the crystal constants in the basal plane and *z*-direction, respectively. In this primitive unit cell there is one B atom and ½ Mg atom with valencies 1 and 2, respectively. Since the π energy gap involves the Mg atoms it follows that $z_\pi = 2$, and since the σ energy gap involves only B atoms we set $z_\sigma = 1$. The ion density parameter, n_0 determines the electron number density, which neutralizes the background ions charge density. Since the π energy gap involves the Mg, and there is ½ such atom in the primitive unit-cell we set $(n_0)_\pi$ = ½, and a similar argument implies that $(n_0)_\sigma = 1$. These choices ignore the different type of bonding associated with the B and Mg atoms. Whereas the Mg atom is bonded (to the B atoms) by releasing its valence electrons, the B atom is bonded (to B atoms) by sharing its valency electrons with its near B neighbor [39]. Notwithstanding this consideration, the choice $(n_0)_\sigma = 1$ in the calculations should be considered as part of our model.

The results of the calculations are displayed in Figure 6)-8). Since our focus is on the $\ell = 6$ symmetry vs. the s-wave symmetry of the π energy gap, only these two symmetries are considered here. Note that, in principle, combinations of different allowable symmetries are also a possibility. For example, recent data suggests a small s-wave admixture to the dominating d-wave symmetry in YBCO [40].

Figure 6) and Figure 7) show two calculations for the ratio of the calculated π energy gap and the experimental values as a function the anisotropy parameter α. The points in the figures are the numerically calculated values, while the lines are a cubic-spline fit to the points. In Figure 6) the $\ell = 6$ symmetry is assumed, while in Figure 7) the s-wave symmetry is assumed.

Comparison of these two calculations for the value of the anisotropy parameter $\alpha \sim 0.83$ suggests that the $\ell = 6$ symmetry is considerably more likely to be the correct one than s wave. This outcome is consistent with the measurements discussed in Section II. Once again we emphasize that there are no adjustable parameters in this calculation. To substantiate our case, the model was also applied for the σ energy gap. We calculated this energy gap assuming both the $\ell = 6$ and s-wave symmetry. These results are shown in Figure 8). For the assumed s-wave symmetry the calculated energy gap is within an order of magnitude of the measured one. On the other hand, for an assumed $\ell = 6$ symmetry there are no nontrivial solutions to the gap equation Eq. (4) . These outcomes strongly indicate that the σ energy gap has s-wave symmetry, consistent with current consensus. It was verified that $\Delta_m^{(1)}(T) \equiv \left|\Delta_m^{(2)}(T)\right|$ in all instances (not shown).

4 Discussion

Given that the nodal hypothesis for the π energy-gap is at odds with the common presumption that the symmetry is s-wave, it is necessary to review the literature that has been used to conclude and support the s-wave symmetry of the π gap This has been done in our previous publications with the conclusion that, to our knowledge, the available data does not settle this issue [3,4,5]. We list this review here, complemented by a comprehensive review of microwave surface-resistance data.

The low-temperature data that was previously checked consisted of tunneling, penetration depth, specific heat, muon-spin rotation, nuclear-spin relaxation ($1/T_1$, Hebel-Schlichter peak), magnetic-field dependence, and the paramagnetic Meissner effect. In this body of data we find that some of it is consistent with a nodal energy gap and some is not. Here we compliment this list by reviewing the available low-temperature surface-resistance data to establish if it is inconsistent with Eq.(3). There are only a very few previous reports in the literature of measurements of the microwave-frequency surface impedance of high-quality thin films of MgB_2. As far as we know there are no reports of single-crystal measurements. In our opinion the existing measurements are not definitive in distinguishing the symmetry of the energy gap. The following discusses the most important of the reported measurements. A definitive result would be demonstration of an exponential dependence of the surface resistance at low temperatures.

Jin *et al.* [41], reported surface resistance measurements on relatively high quality thin films and reported an exponential low-temperature dependence, $R_s(T) \propto e^{-\Delta(T)/kT}$ as in Eq (2). However the reported fitting parameter is $\Delta(T=0) = 3.4$ meV, which disagrees with the accepted values of 2-2.3 meV for the π gap, which dominates the low-temperature behavior.

Zaitsev *et al*. [42] reported a fit to exponential dependence over a wide range of temperatures, but as they point out in the paper, the statistical errors in the measurements preclude a definitive conclusion of of s-wave behavior.

Hakim *et al.*[43] reported a fit to an s-wave exponential dependence over the entire temperature range. The film was reported to be a mixture of textured MgO and nanocrystalline MgB_2, with grain sizes ~ 5 nm and $T_C = 31$ K. While such a film and this result is of interest in the context of a prediction that heavy doping of MgB_2 results in a one-gap high-T_C superconductor, this data does not pertain to the clean-limit high-quality films under study.

Moeckly *et al.* [44] reported measurements on a film made by the same-reactive evaporation technique as we have in our publications [3,4,5] using, however, a parallel plate resonator as opposed to the stripline resonator that we have employed. The results showed what appeared to be sharp decrease at low temperature that resembled exponential behavior but without further analysis to fit and extract a value for the energy gap. We point out that the parallel-plate-resonator result required subtraction of "background losses" that may have increased the uncertainty of the measurements. We also note that the paper also reports measurements made in our laboratory on similar films (as we have reported in our papers and in Section II) that follow a power-law behavior at low temperatures.

Cifariello *et al.* [45] have measured the IMD in high-quality MgB_2 films. Their measurements did not show an upturn in IMD at the temperatures range $T/T_c > 0.2$. In so measuring they missed the region with the strongest evidence of the upturn where $T/T_c < 0.2$, see Fig. (1).

To conclude this survey of microwave-frequency surface-impedance measurements, we assert that the literature on this topic, to the best of our knowledge, contains only inconclusive evidence for s-wave symmetry.It is worthwhile to point out that there have been also low-temperature reports of penetration depth measurements that indicate unconventional superconductivity [46, 47, 48 49, 50). In those works, however, the explicit energy-gap functional form has not been specified.

Note that given our conclusion about the π energy-gap symmetry, we have in MgB_2 an interesting configuration where the symmetry of the σ energy gap (s-wave) and that of the π energy gap (i-wave) are different. This configuration may not be unique to MgB_2. We note that the superconductors 2H-$NbSe_2$ and $NbSe_3$ share the same crystal structure, both have two energy gaps, and comprise alternating Nb and Se layers analogous to the B and Mg layers in MgB_2 [51], This suggests that low temperature measurements of the penetration depth, surface resistance and intermodulation distortion 2H-$NbSe_2$ and $NbSe_3$ would be of great interest.

5 Summary

We have presented a phenomenological model for calculating the energy gaps in MgB_2 at $T = 0$ K. The model is an extension of the BCS theory to account for both the coulomb repulsion and the considerable anisotropy in the elastic properties. The calculations support our previous hypothesis that the π energy gap is nodal, with six nodal lines $\boldsymbol{\ell} = 6$ (I wave in spectroscopic notation), in contrast to the common assumption that the π gap is conventional s wave. Our calculations are also consistent with the common viewpoint that the σ energy gap has conventional s-wave symmetry. The calculations assume a Fermi surface that comprises of two sheets each underlying a separate energy gap [10], and no coupling between the phonons and electron seas that pertain to the two gaps. All the required input parameters for the model are available from independent data and calculations in the literature. Given that the gap equation is highly nonlinear (Eqs.(4) and (B.10)) this outcome substantiates the self-consistency of the input parameters (Table 2).

We have also presented a new analysis of recently published measurements of the surface resistance in MgB_2 [6]. This data clearly exhibit non-exponential decay at low-temperatures, a feature inconsistent with an s-wave π gap. Our analysis shows that, in fact, the measured low-temperature dependence of surface resistance follows a power law, as would be expected for a nodal energy gap. This result is further substantiated by a survey of the literature on measurements of the low-temperature surface-impedance variation that leads to the conclusion that there is no unambiguous evidence for the exponential dependence as predicted by an s-wave symmetry.

All of the findings here support strongly our previous hypothesis, based on our measurements, that the π energy gap is nodal with $\boldsymbol{\ell} = 6$, six nodal lines.

Acknowledgments

We would like to acknowledge the support of the Naval Surface Warfare Center, Carderock Division, Bethesda MD. Y.D.A. acknowledges financial support from MIT Lincoln Laboratory. This material is based upon work supported by the Department of the Navy under Air Force Contract No. FA8721-05-C-0002 and/or FA8702-15-D-0001. Any opinions, findings, conclusions or recommendations expressed in this material are those of the author(s) and do not necessarily reflect the views of the Department of the Navy.

We thank Dr. C. E. Reece of Jefferson Laboratory for sharing his raw data with us.

Appendix A

The Phonon-Induced Attractive Interaction $V_{PH}(\vec{q})$, Eq.(8)

Equation Section (Next)The parametrization of the $V_{PH}(\vec{q})$ is motivated by the corresponding expression for an isotropic superconductor, Eq.(6). Consider two limits of the momentum exchange, i.e., in the $\perp$ and $\square$ directions, and assume that in (6) the only direction-dependent factor in the amplitude is v_{SOUND}. For these special instances we would write

$$\gamma(\vec{q}_{\perp})=\frac{\tilde{\gamma}}{v_{SOUND}(\vec{q}_{\perp})},\quad \gamma(\vec{q}_{\square})=\frac{\tilde{\gamma}}{v_{SOUND}(\vec{q}_{\square})},\quad \tilde{\gamma}=\left(\frac{4\pi z\, e^2}{q_{TF}^2}\right)\left(\sqrt{\frac{n_0}{M}}\right) \tag{A.1}$$

Consequently, a convenient expression that applies to all $\vec{q}$ directions and coincides with the two limits in Eq.(A.1) is the interpolation

$$\frac{1}{v_{SOUND}}\rightarrow\frac{1}{v_{SOUND}(\vec{q})}=\sqrt{\frac{q_{\square}^2+q_{\perp}^2}{\left(v_{SOUND}(\square)\,q_{\square}\right)^2+\left(v_{SOUND}(\perp)\,q_{\perp}\right)^2}} \tag{A.2}$$

where

$$\left(\frac{1}{v_{SOUND}(\vec{q})}\right)^2=\left(\frac{1}{v_{SOUND}(\perp)}\right)^2\frac{1}{1+\alpha\left(\frac{q_{\square}^2}{q^2}\right)},\qquad q^2=q_{\square}^2+q_{\perp}^2,$$

$$\alpha=\left(\frac{v_{SOUND}(\square)}{v_{SOUND}(\perp)}\right)^2-1. \tag{A.3}$$

Since the π - gap involves vibrations of the B and Mg planes against each other, i.e., in the $\perp$ direction, and employing (A.3) we write

$$V_{PH}(\vec{q})=-\frac{\gamma_{\pi}^2}{1+\alpha\left(\frac{q_{\square}^2}{q_{\square}^2+q_{\perp}^2}\right)}\qquad \gamma_{\pi}=\frac{\pi^2(\hbar c)^3\,z(n_0)}{\left(m^*c^2\right)^2\left(\frac{v_F}{c}\right)\sqrt{B(\perp)}} \tag{A.4}$$

In (A.4) we used the substitutions mentioned after Eq.(6). By the same token, since the σ -gap is associated with in-plane B vibrations in the □ direction, we arrive at

$$V_{PH}\left(\vec{q}\right) = -\frac{\gamma_{\sigma}^{2}}{1+\alpha\left(\frac{q_{\square}^{2}}{q_{\square}^{2}+q_{\perp}^{2}}\right)} \qquad \gamma_{\sigma} = \frac{\pi^{2}\left(\hbar c\right)^{3} z\left(n_{0}\right)}{\left(m^{*}c^{2}\right)^{2}\left(\frac{v_{F}}{c}\right)\sqrt{B(\square)}}\sqrt{\frac{v_{SOUND}\left(\perp\right)}{v_{SOUND}\left(\square\right)}} \tag{A.5}$$

In Eqs.(A.4),(A.5), the symbols $B(\perp), B(\square)$ denote the bulk moduli in the $\perp$ direction and the □ plane, respectively (dimensionality $[\boldsymbol{B}] = \boldsymbol{\mathcal{E}}\ell^{-3}$). For the hexagonal-crystal-structure the elastic constants are given by [52,53]

$$B(\square) = \frac{\Lambda}{2+\alpha_{R}}, \qquad B(\perp) = \frac{\Lambda}{\alpha_{R}\left(2+\alpha_{R}\right)}$$
$$\alpha_{R} = \frac{C_{1,1}+C_{1,2}-2C_{1,3}}{C_{3,3}-C_{1,3}}, \qquad \Lambda = 2\left(C_{1,1}+C_{1,2}\right)+4C_{1,3}\,\alpha_{R}+C_{3,3}\,\alpha_{R}^{2}, \tag{A.6}$$

where the two moduli in Eq.(A.6) obey the relation

$$\frac{1}{B(\square)}-\frac{1}{B(\perp)} = \frac{C_{3,3}-C_{1,1}-C_{1,2}+C_{1,3}}{C_{3,3}\left(C_{1,1}+C_{1,2}\right)-2C_{1,3}^{2}} \tag{A.7}$$

Appendix B

Multipole Expansions and the Gap Equation, Eq.(4).

Equation Section (Next)

To solve the gap equation, Eq.(4), it is necessary to specify the band structure and deal with the required three-dimensional integration. These matters are detailed in this Appendix to facilitate reproduction of our calculations if needed.

Consider first the band structure. *Ab-initio* band-structure calculations yield two π Fermi-surface sheets (an electron-like and a hole-like), adjacent to the Brillouin zone facets and of complicated topology, and two nesting σ tube-like Fermi surface sheets (hole like) aligned with the Γ-A line [9,54, 55]. In our calculations we consider only one Fermi sheet for each energy-gap .For the π Fermi-surface sheet we approximate the hexagonal Brillouin zone by a cylinder of radius $K_F(\pi)$ and half-height $k_{BZ}=\pi/a_C$. The maximum and minimum lateral extensions of the hexagonal Brillouin-zone geometry, suggest that $\frac{2\pi}{\sqrt{3}\,a_a}<K_F(\pi)<\frac{4\pi}{3a_a}$ where a_a is the lattice constant in the $\hat{x}$ direction. In that Brillouin zone cylinder, the π Fermi-surface sheet extends over about half the Brillouin-zone height. Since we average the gap equation over the k_Z variable, see below, we use for that sheet the entire Brillouin-zone height. For the σ energy gap, the chosen Fermi surface is a single tube with an averaged radius $K_F(\sigma)$ [56]. These considerations suggest the following approximate band energies

$$\varepsilon_\pi(K,k_Z)\approx\frac{\hbar^2K^2}{2m^*_\pi},\quad \varepsilon_\sigma(K,k_Z)\approx\frac{\hbar^2K^2}{2m^*_\sigma},\quad and\quad K\le K_F(\pi,\sigma)\quad -\frac{\pi}{a_C}\le k_Z\le\frac{\pi}{a_C},\quad \text{(B.1)}$$

and $m^*_\pi, m^*_\sigma, K_F(\pi,\sigma)$ are effective masses of the π and σ Fermi surfaces. These are available from data and band-structure calculations [56,57].

Eq.(B.1) implies that $\xi(\vec{k})\approx\xi(K)$ and that

$$\left|\vec{q}_{\square}\right| = \left|\vec{K} - \vec{K}'\right| \cong K_F \sqrt{2\left(1-\cos\left(\varphi-\varphi'\right)\right)} \tag{B.2}$$

where φ,φ' are the basal azimuthal angles of $\vec{K},\vec{K}'$, respectively, and K_F is the pertaining basal Fermi momentum in the cylindrical coordinate system.

To carry out the integrations implied by (4) the multipole expansions of the interactions are required. These are

$$\left.\begin{aligned} V_{PH}\left(\vec{q}\right) &= \sum_{m=0}^{\infty} V_{PH}^{(|m|)}\left(q_{\perp}\right)\cos\left(m\left(\varphi-\varphi'\right)\right) f_m \\ V_{C}\left(\vec{q}\right) &= \sum_{m=0}^{\infty} V_{C}^{(|m|)}\left(q_{\perp}\right)\cos\left(m\left(\varphi-\varphi'\right)\right) f_m \end{aligned}\right\} \quad f_m = 2-\delta_{m,0} \tag{B.3}$$

where m denotes the multipole order and

$$V_{PH}^{(|m|)}\left(q_{\perp}\right) = \left(\frac{f_m}{2\pi}\right)\times\int_0^{2\pi} d\varphi\cos\varphi\left(\frac{1-\cos\varphi+a^2}{\left(1+\alpha\right)\left(1-\cos\varphi+a^2\right)}\right) =$$

$$= \left(\frac{f_m}{2\pi}\right)\left(\delta_{m,0}\left(\frac{2\pi}{1+\alpha}\right)+\left(\frac{2\pi|a|\alpha}{\left(1+\alpha\right)\sqrt{2+2\alpha+a^2}}\right)\left(\frac{1+\alpha+a^2-|a|\sqrt{2+2\alpha+a^2}}{1+\alpha}\right)^{|m|}\right),$$

$$V_{C}^{(|m|)}\left(q_{\perp}\right) = \left(\frac{f_m}{2\pi}\right)\times\int_0^{2\pi} d\varphi\cos\varphi\left(\frac{1}{1-\cos\varphi+b^2}\right) = \left(\frac{f_m}{2\pi}\right)\times\left(\frac{2\pi}{|b|\sqrt{2+b^2}}\right)\left(1+b^2-|b|\sqrt{2+b^2}\right)^{|m|},$$

$$a^2 = \frac{q_{\perp}^2}{2K_F^2} \qquad b^2 = \left(\frac{1}{2K_F^2}\right)\left(q_{\perp}^2+q_{TF}^2\right)$$

(B.4)

According to Eq.(11), only the multipoles m=0,3,6, are possible,.

We turn now to the RHS of the gap equation (4), which we denote here by $F\left(\vec{k}\right)$. For the approximate band energy of Eq.(B.1) we have

$$\int d\vec{k}\,' F\left(\xi\left(\vec{K}'\right), \mathrm{k}_Z - \mathrm{k}_Z', \varphi - \varphi'\right) \cong \left(\frac{m^*}{\hbar^2}\right) \int_{-\pi/a_C}^{\pi/a_C} d\mathrm{k}_Z' \int_{-\infty}^{\infty} d\xi' \int_0^{2\pi} d\varphi' F\left(\xi', \mathrm{k}_Z - \mathrm{k}_Z', \varphi - \varphi'\right) \quad \text{(B.5)}$$

The triple integration in Eq.(B.5) becomes tractable since the φ', ξ' integrations are available analytically, and the φ', ξ' and the k_Z' variables are separable.

Consider first the angular integration. For s-waves ($m = 0$) the φ integration in is trivial. For $m > 0$ the angular integration gives rise to the integral

$$\int_0^{2\pi} d\varphi \frac{\sin^2(6\varphi)}{\sqrt{\xi^2 + \Delta^2 \sin^2(6\varphi)}} = \int_0^{2\pi} d\varphi \frac{\sin^2(3\varphi)}{\sqrt{\xi^2 + \Delta^2 \sin^2(3\varphi)}} = \int_0^{2\pi} d\varphi \frac{\cos^2(3\varphi)}{\sqrt{\xi^2 + \Delta^2 \cos^2(3\varphi)}} =$$
$$= \left(\frac{4|\xi|}{\Delta^2}\right)\left(E\left(-\frac{\Delta^2}{\xi^2}\right) - K\left(-\frac{\Delta^2}{\xi^2}\right)\right), \quad \text{(B.6)}$$

where the symbols E, K denote the complete elliptic integrals of the first and second kinds, respectively [58,59].

The ξ' integration in Eq.(4) is limited by the step functions in Eqs.(5),(11). This integration yields

$$G^{(0)}\left(\frac{u}{\Delta}\right) = (2\pi)\int_0^u d\xi \frac{1}{\sqrt{\xi^2 + \Delta^2}} = (2\pi)\,Log\left(\frac{u + \sqrt{u^2 + \Delta^2}}{|\Delta|}\right) \quad for\ m = 0$$
$$G^{(m)}\left(\frac{u^2}{\Delta^2}\right) = \int_0^u d\xi \left(\frac{4|\xi|}{\Delta^2}\right)\left(E\left(-\frac{\Delta^2}{\xi^2}\right) - K\left(-\frac{\Delta^2}{\xi^2}\right)\right) \qquad for\ m = 3, 6. \quad \text{(B.7)}$$

The analytic expression for $G^{(m)}$ involves the Meijer G functions is not quoted here. Carrying the ξ' and φ' integrations results in that the φ, ξ dependencies on both sides of the gap equation, Eq.(4), cancel out exactly, as they should.

The last k_Z integration, Eq. (11), is done numerically. For the two symmetries considered in this work $f_\Gamma(k_Z) = 1$. The final equations for the two unknowns $\Delta_m^{(1,2)}(T)$ in Eq.(11) are

obtained by averaging both sides of the gap equation (4) over the Brillouin zone k_Z coordinate [36]. This step gives rise to the form factors

$$A_{PH,C}^{(m)} = \int_0^{\pi/a_C} \int_{-\pi/a_C}^{\pi/a_C} dk_Z dk_Z' V_{PH,C}^{(m)}\left(k_Z - k_Z'\right) \Big/ \int_0^{\pi/a_C} dk_Z \,. \tag{B.8}$$

It is convenient to express the ensuing equations in terms of dimensionless unknowns. For this purpose we introduce the following variables

$$\hbar\tilde{\omega}_{D,P} = \frac{\hbar\omega_{D,P}}{\Delta\left(T=0K\right)}, \quad \tilde{\Delta}_m^{(1,2)} = \frac{\Delta_m^{(1,2)}}{\Delta\left(T=0K\right)}, \tag{B.9}$$

where $\Delta\left(T=0K\right)$ is the pertaining measured energy-gap (π or σ). Putting all these pieces together, the coupled nonlinear equations for the unknowns $\tilde{\Delta}_m^{(1,2)}$ are

$$\begin{aligned}
\tilde{\Delta}_m^{(1)} &= +\frac{f_m}{\left(2\pi\right)^3}\left(\frac{m_{\pi,\sigma}{}^* c^2}{\left(\hbar c\right)^2}\right)\gamma_{\pi,\sigma}^2\, A_{PH}^{(m)}\, G^{(m)}\left(\left(\frac{\hbar\tilde{\omega}_D}{\tilde{\Delta}_m^{(1)}}\right)^2\right)\tilde{\Delta}_m^{(1)} + \tilde{\Delta}_m^{(2)} \\
\tilde{\Delta}_m^{(2)} &= -\frac{f_m}{\left(2\pi\right)^3}\left(\frac{m_{\pi,\sigma}{}^* c^2}{\left(\hbar c\right)^2}\right)\gamma_C^2\, A_C^{(m)}\left(\tilde{\Delta}_m^{(1)}\, G^{(m)}\left(\left(\frac{\hbar\tilde{\omega}_D}{\tilde{\Delta}_m^{(1)}}\right)^2\right) + \tilde{\Delta}_m^{(2)}\left(G^{(m)}\left(\left(\frac{\hbar\tilde{\omega}_P}{\tilde{\Delta}_m^{(2)}}\right)^2\right) - G^{(m)}\left(\left(\frac{\hbar\tilde{\omega}_D}{\tilde{\Delta}_m^{(1)}}\right)^2\right)\right)\right).
\end{aligned} \tag{B.10}$$

The coupled equations (B.10)are solved by searching for a solution over a 'reasonable' range of the $\tilde{\Delta}_m^{(1,2)}$ unknowns. In some instances there are no solutions except for the trivial one $\tilde{\Delta}_m^{(1,2)} = 0$.

Table 1. The allowed positive-parity energy-gap symmetries for hexagonal crystal structure*

Symmetry notation	Energy gap $\Delta\left(\vec{k}\right)$
Γ_1^+	$\Delta_0(T),\quad \Delta_0(T)\dfrac{K^2}{K_{BZ}^2},\quad \Delta_0(T)\dfrac{k_Z^2}{k_{BZ}^2}$
Γ_2^+	$\Delta(\varphi;T)=\Delta_0(T)\sin(6\varphi)$
Γ_3^+	$\Delta(\varphi;T)=\Delta_0(T)\dfrac{k_Z}{k_{BZ}}\times\begin{cases}\sin(3\varphi)\\ \cos(3\varphi)\end{cases}$

∗ The symbols K_{BZ} and k_{BZ} denote the momentum extensions of the first Brillouin zone in the basal plane and z directions, respectively. These arbitrary normalizing constants are introduced so that the energy-gap amplitude $\Delta_0(T)$ has dimension of energy.

Table 2. The parameters employed in Eq.(8)*

Parameter	π Energy Gap	σ Energy Gap	Reference
$< v_F >/c$	0.00161	0.00146	60,54
z	1/2	1	See text
$n_0 V_{UC}$ (nm^3)	2	1	See text
B (GPa)	B(⊥)=279.07	B(‖)=587.78	Eqs. (12),(A.6)
m^*/m_0	0.375	0.9	1,25,57
Δ(T=0 K)(eV)	0.002	0.0071	1,2,37
$K_F(nm^{-1})$	10.018	3.34	1,2,37

* $V_{UC} = .0.25\ a_a^2 a_c \sqrt{3}$ is the primitive unit-cell volume, where we used a_a=0.3086 nm , a_c = 0.3524 nm [1]. Other parameters used in the calculations are: $\hbar\omega_D = 750\, k_B$ where k_B is the Boltzmann constant [37, 55], $\hbar\omega_P = 7\, eV$, Δ_π= 0.002 eV, Δ_σ = 0.007 eV [1,9], $q_{TF} = 0.7\ (a_B)^{-1}$ where a_B denotes the Bohr radius[54], $\hbar c = 197.3\,\text{eV}\times\text{nm}$.

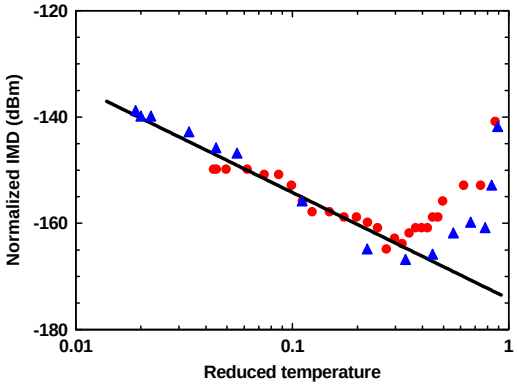

Figure 1 Normalized IMD vs reduced temperature T/T_c ▲ for typical YBCO[12], and ● for MgB_2 [3]. Solid line is a $1/T^2$ dependence. The similarity between YBCO and MgB_2 is an indication that the energy gap in MgB_2 contains nodes.

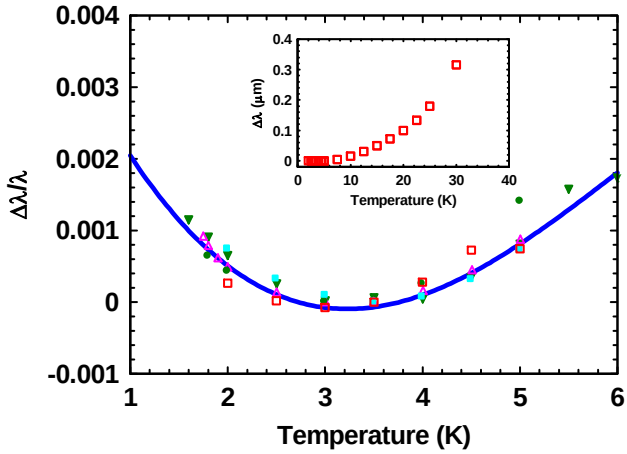

Figure 2. Main plot: $\Delta\lambda/\lambda$ vs. temperature for MgB_2 very low temperatures [4]. The inset shows the same quantities over the entire temperature range < T_c. Several samples are shown. All demonstrate the increase at low temperatures attributed to Andreev bound states [4]. This increase is only visible on the expanded scale of the main plot.

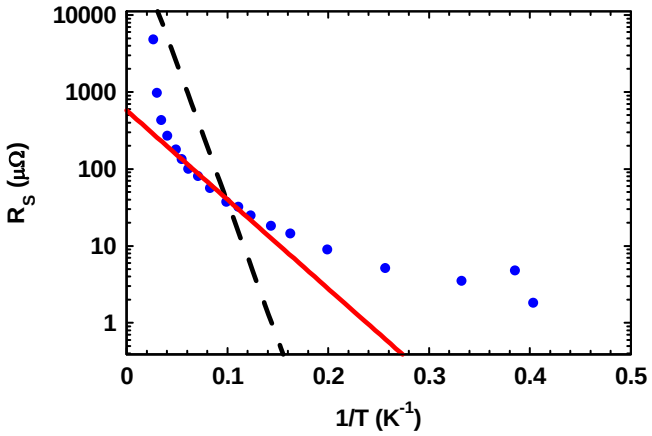

Figure 3. Semilog plot of $R_s = R_{Measured} - R_{RES}$ vs. $1/T$, where $R_{Measured}$ denotes the measured effective surface resistance of the 350nm film by the JLab group [6] and R_{RES} is defined as the temperature independent value of surface resistance at low temperatures. The solid (red, in the online version) and dashed (black, in the online version) are plots of $e^{-\Delta/kT}$ where Δ are accepted values for MgB_2, $\Delta_\pi = 2.3$ meV and $\Delta_\sigma = 7.1$ meV, respectively. Neither value fits the data.

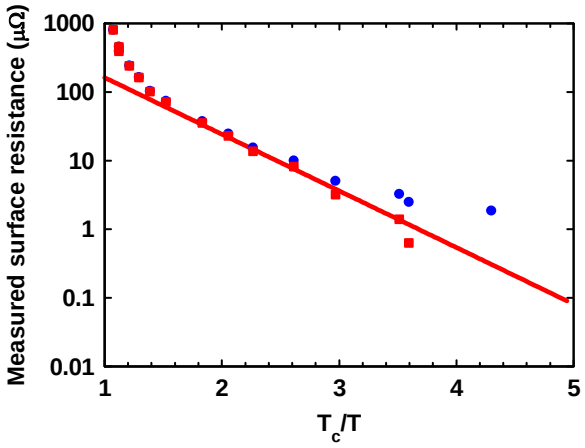

Figure 4**.** Semilog plot of measured niobium surface-resistance vs T_C/T from JLab [6]. ● is $R_{Measured}$ values, ■ $R_{Measured} - R_{RES}$. Solid line (red in online version) is Eq. (2) with the accepted value of for the niobium energy gap, $\Delta = 1.5$ meV, which fits the data over two orders of magnitude.

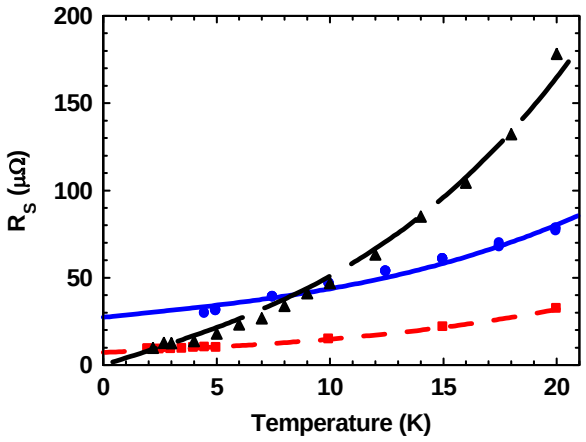

Figure 5. R_S vs T of the JLAB data [6] and stripline resonator measurements at Lincoln Laboratory of MgB_2 deposited by reactive evaporation [22]. All data are scaled by f^2 to 7.4 GHz. ▲ measurements of the 350-nm thick film from JLab, ■ stripline-resonator measurement at Lincoln Laboratory of film deposited by reactive evaporation and ● stripline resonator measurements at Lincoln Laboratory of MgB_2 deposited by HPCVD. The lines are best fits to the various data sets with the expression in Eq. (3) with $\Delta_\pi = 2.3$ meV, or explicitly $R_S = A(T/T_C + .0026(T/T_C)^3) + B$, where A and B are taken as free parameters. The values of A and B are as follows: for the long-dashed line A = 4.04 and B = 3.87x10^{-8}; for the solid line A = 1.30 and B = 27.3; and for the short-dashed line A = 0.607 and B = 7.13 in the proper units.

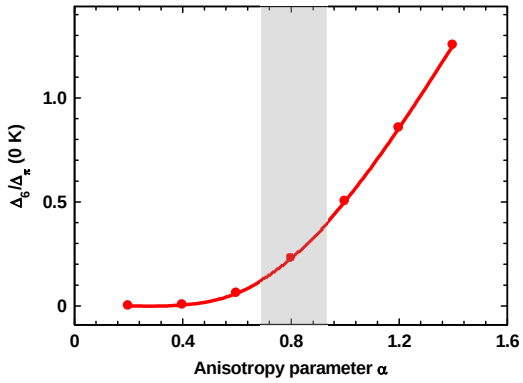

Figure 6. Ratio of the calculated π energy gap for the $\ell = 6$ symmetry Δ_6 and the representative experimental value $\Delta_\pi = 2$ meV vs. the anisotropy parameter α Eq.(9). The shaded region depicts the range of experimentally determined anisotropy parameters. The points are the numerically calculated values and the line is a spline fit to the points. The calculated Δ_6 is within an order of magnitude of the experimental value.

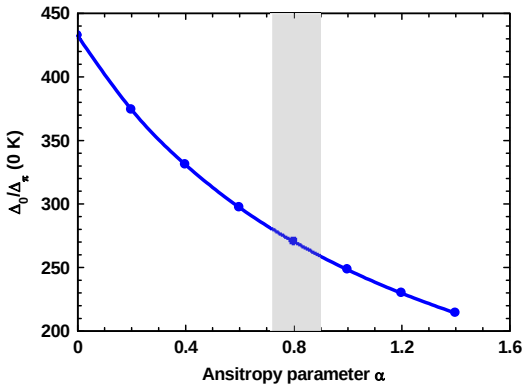

Figure 7 Ratio of the calculated π energy gap for the $\ell = 0$ symmetry, Δ_0 and the experimental value $\Delta_\pi = 2$ meV vs. the anisotropy parameter α Eq. (9). The shaded region depicts the range of experimentally determined anisotropy parameters. This calculated result disagrees with the experimental result y two oders of magnitude. Together with Figure 6 this leads to the conclusion that the $\ell = 6$ symmetry is much more likely for the π gap. The points are the numerically calculated values and the line is a spline fit to the points.

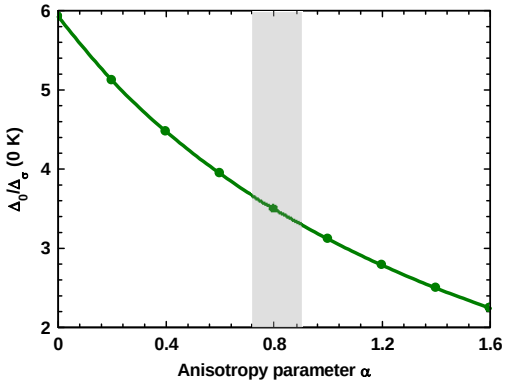

Figure 8. Ratio of the calculated σ energy gap for the $\ell = 0$ symmetry, Δ_0 and the experimental value $\Delta_\sigma = 7$ meV vs. the anisotropy parameter α Eq. (9). The shaded region depicts the range of experimentally determined anisotropy parameters. There is no nontrivial solution for the case of $\ell = 6$ symmetry. The calculated result is within an order of magnitude of the experimental value. This indicates that the σ gap is likely a conventional s-wave symmetry. The points are the numerically calculated values and the line is a spline fit to the points.

6 References

[1] X. X. Xi, Rep. Prog. Phys. 71 (2008) 116501; C. Zhuang ; T. Tan; A Krick,.; Q. Lei; K.Chen; X.X. Xi, J. Superconduct. and Novel Mag.,26, (2013) 1563,
[2] A. Floris *et al*., Physica C 456 (2007) 45; C. Buzea, T. Yamashita, Superconductivity Sci. Tech. 14 (2001) R115.
[3] Y. D. Agassi, D. E. Oates, B. H. Moeckly Phys. Rev. B 80 (2009) 174522.
[4] Y. D. Agassi, D. E. Oates, B. H. Moeckly Physica C 480 (2012) 79.
[5] Y.D. Agassi, D.E. Oates Physica C 506 (2014) 119.
[6] B. P. Xiao, X. Zhao, J. Spradlin, C. E. Reece, M. J. Kelly, T. Tan, X. X. Xi, Supercond. Sci. Technol. 25 (2012) 095006.
[7] A. S. Alexandrov, Phys. Rev. B **77** (2008) 094502.
[8] N. N. Bogoliubov,V. V. Tolmachev, D. V. Shirkov, A New Method in the Theory of Superconductivity, Chapman & Hall Ltd., London, 1959.
[9] P. C. Canfield, G. W. Crabtree Physics Today, 56 (2003) 34.
[10] H. J. Choi, D. Roundy, H. Sun, M. L. Cohen, S. G. Louie Nature 418 (2002) 758.
[11]H. J. Choi, M. L. Cohen and S, G. Louie, Physica C 385 (2003) 66.
[12] D. E. Oates, S.-H. Park, G. Koren, Phys. Rev. Lett. 93 (2004) 197001.
[13] T. Dahm D. J. Scalapino, J. Appl. Phys. 81 (1997) 2002.
[14] D. Agassi D. E. Oates, Phys. Rev. B 72 (2005) 014538.
[15] H.Walter *et al*., Phys. Rev.Lett.80 (1998) 3598; L. Alff *et al*., Europ. Phys. J. 5 (1998) 423
[16] L. Alff et al., Europ. Phys. J., 5 (1998) 423
[17] A. A. Abrikosov, Fundamentals of the Theory of Metals, North-Holland, Amsterdam, 1988, p 364
[18] R. Vaglio, RF Superconducting Cavities for Accelerators, in H Weinstock and M Nisenoff (Eds.), Microwave Superconductivity, Kluwer Academic Publishers, Dordrecht, 2001.
[19] H. Padamsee, J. Knobloch, T. Hays, RF Superconductivity for Accelerators, Wiley & Sons, New York, 1998.
[20] M. Iavarone et al., Phys. Rev. B 71 (2005) 214502.
[21] T. Van Duzer and C. W. Turner, Superconductive Devices and Circuits, Second Edition, Prentice Hall PTR, Upper Saddle River, NJ, 1999, p 132.
[22] D. E. Oates, Y. D. Agassi, B. H. Moeckly, IEEE Trans. Appl. Supercond. 17 (2007) 2871; D. E. Oates, Y. D. Agassi, B. H. Moeckly, Supercond. Sci. Technol. 23 (2010) 034011.
[23] B. H. Moeckly, W. S. Ruby, Supercond. Sci. Technol. 19 (2006) L21.
[24] J.R. Kirtley, C.C Tsuei, M Rupp, J.Z Sun, L.S Yu-Jahnes, A Gupta, M.B Ketchen; K.A. Moler, M. Bhushan, Phys. Rev. Lett. 76 (1996) 1336.
[25] I. I. Mazin, J. Kortus, Phys. Rev. B 65, 180510(R) (2002).
[26] I.I. Mazin et. al. , Phys. Rev. Lett. 89 (2002) 107002.
[27] H. Suhl, B. T. Matthias, L. R. Walker, Phys. Rev. Lett. 3 (1959) 552
[28] J. B. Ketterson and S. N. Song, Superconductivity, Cambridge University press, Cambridge, U.K.,1999.
[29] M.Tinkham, Introduction to Superconductivity, fourth ed., Dover Publications, Mineola, NY, 1996.
[30] I. N. Askerzade, Uspechi 52 (2009) 977
[31] A. L. Fetter and J. D. Walecka, Quantum Theory of Many-Particle Systems, McGraw-Hill, New York, 1971, p. 475-476.
[32] A. L. Fetter and J. D. Walecka, *op. cit.* p. 401.
[33] C. Kittel, Introduction to Solid State Physics, fourth ed., John Wiley and Sons, New York, 1971, Chap. 4
[34] A. B. Auld, Acoustic Fields and Waves in Solids, Vol. I, John Wiley & Sons, New York, 1973, pp.389; H. M. Ledbetter, J. Phys. Chem. Data, 6 (1977) 1181.
[35] K. Chen, W. Dai, C. G. Zhuang, Li, Carabello, lambert, Mlack, Ramos, Xi, Nature Communications 3 (2012) 619.
[36] . M. Sigrist, K. Ueda, Rev. Mod. Phys., 63, 239 (1991), 247.
[37] S. L. Budko and P. C. Canfield, Physica C 514 (2015) 142.
[38] I. R. Shein A. L. Ivanovskii, J. Phys. 20 (2008) 415218, and references therein.
[39] I. I. Mazin and V. P. Andropov, Physica C 385 (2003) 49.
[40] Yu. A. Nefydov et al.,Physica B 284-288 (2000) 919

[41] B B Jin, N Klein, W N Kang, Hyeong-Jin Kim, Eun-Mi Choi, Sung-I K Lee, T Dahm and K Maki, Supercond. Sci. Technol. 16 (2003) 205
[42] A.G. Zaitsev, R. Schneider, R. Hott, F. Ratzel, G.Linker, J. Geerk, Institute of Physics Publishing J. of Physics: Conference Series 43 (2006) 309.
[43] N. Hakim, C. Kusko, S. Sridhar, A. Soukiassian, X. H. Zeng, X. X. Xi, Appl. Phys. Lett. 81 (2002) 3603.
[44] Brian H. Moeckly, Ken E. Kihlstrom, Alp T. Findikoglu, Dan E. Oates, IEEE Trans. Appl. Superconduct., 15 (2005) 3308.
[45] G. Cifariello, M. Aurino, E. Di Gennaro, G. Lamura, A. Andreone, P. Orgiani, X. X. Xi, and J.-C. Villégier Appl. Phys. Lett. 88, 142510 (2006).
[46] C. Panagopoulos, B.D. Rainford, T. Xiang, C.A. Scott, M. Kambra, H. Inoue, Phys. Rev. B 64 (2001) 094514.
[47] A. V. Pronin, A. Pimenov, A. Loidl, S.I. Krasnosvobodtsev, Phys. Rev. Lett. 87 (2001) 097003.
[48] N. Klein, B.B. Jin, J. Shubert, M Schuster, H.R. Yi, A Pinenov, A Loidl, S.I. Krasnosvobodtsev arXiv:cond-mat/0107259v1.
[49] R. Jin, M. Paranthaman, H. Y. Zhai, H. M. Christen, D. K. Christen, D. Mandrus, Phys. Rev. B 64 (2001) 220506(R).
[50] M. Moarrefi-Romeileh, H.Yavari, A.A.Joata-bayrami, M.R.Abolhassani, Physica B 406 (2011) 4135
[51] M. Marz, G. Goll, W. Goldacker, R. Lorz, Phys. Rev. B 82 (2010) 024507; J. Kacmarcick, Z. Pribulova, C. Marcenat, T. Klein, P. Rodiere, L. Cario, P. Samuely, Phys. Rev. B 82 (2010) 014518; J. D. Fletcher, A. Carrington, P. Diener, P. Rodiere, J. P. Brison, R. Prosorov, T. Ohlheiser, R. W. Giannetta, Phys. Rev. Lett. 98 (2007) 057003; V. Guritanu, W. Goldacker, F. Bouquet, Y. Wang, R. Lorz, G. Groll, A. Junod, Phys. Rev. B 70 (2004) 184526.
[52] P. Ravindran, P. Vajeeston, R. Vidya, A. Kjekshus, H. Fjellvag, Phys. Rev. B 64 (2001) 224509.
[53] G. Steinle-Neumann, L. Strixrude, R. E. Cohen, Phys. Rev. B, 60 (1999) 791.
[54] J. Kortus, I. I. Mazin, K. D. Belashchenko, V. P. Antropov, L. L. Boyer, Phys. Rev. Lett., 86 (2001) 4656.
[55] S. V. Shulga, S. I. Drechsler, H. Eschrig, H. Rosner, W. Pickett, arXiv: cond-matter/0103154v1 (2002)
[56] J. M. An, W. E. Pickett, Phys. Rev. Lett., 86 (2001) 4366.
[57] E. A. Yelland, J. R. Cooper, A. Carrington, N. E. Hussey, P. J. Meeson, S. Lee, A. Yamamoto, S. Tajima, Phys. Rev. Lett. 88 (2002) 217002; A. Carrington, P. J. Meeson, J. R. Cooper, L. Balicas, N. E. Hussey, E. A. Yelland, S. Lee, A. Yamamoto, S. Tajima, S. M. Kazakov, J. Karpinski, 91 (2003) 037003.
[58] G. B. Arfken, H. J. Weber, Mathematical Methods for Physicists, Sixth ed., Elsevier, Amsterdam, 2005, pp. 370.
[59] L. M. Milne-Thomson, Elliptic Integrals, in M. Abramowitz and I. A. Stegun eds. Handbook of Mathematical Functions, National Bureau of Standards, Washington, DC, 1964, pp. 589-591.
[60] A. Brinkman, A. A. Golubov, H. Rogalla, O. V. Dolgov, J. Kortus, Y. Kong, O. Jepsen, O. K. Andersen, Phys. Rev. B 65 (2002) 180517(R).